Structures 67 (2024) 106960

Contents lists available at ScienceDirect

Structures

journal homepage: www.elsevier.com/locate/structures

Conceptual study of an innovative friction damper for the seismic retrofit of precast RC structures with poor connections

Eleonora Grossi [a,*], Matteo Zerbin [a], Alessandra Aprile [a], Raffaele De Risi [b], Flavia De Luca [b]

[a] University of Ferrara, Ferrara, Italy
[b] University of Bristol, Bristol, UK

ARTICLE INFO

Keywords:
Precast RC structure
Friction damper
Conceptualisation
Seismic performance
Importance analysis

ABSTRACT

Precast RC structures have been widely used in industrial and commercial buildings since the 60 s in the most developed areas. However, during those decades of economic growth, most buildings were constructed without seismic design criteria, accounting for gravity loads only. For this reason, this structural typology often faces a significant seismic risk in earthquake-prone areas due to the lack of effective connection between structural elements. As a result, the seismic retrofit of precast RC structures is essential to prolong their service life and mitigate seismic losses. The present work shows the conceptualisation study of an innovative seismic protection device called Bidirectional Rotational Friction Damper (BRFD) for precast RC structures that behave simultaneously as a beam-to-column joint and damper. This device unifies the concepts of rotational friction dampers and a movable plate system, producing a damping effect along two main directions. Furthermore, the device's ability to dissipate energy through friction enables it to remain undamaged during multiple seismic events while maintaining its damping capacity. After defining a simplified analytical model, to evaluate the influence of the BRFD on a structure's behaviour during a seismic event, a case study was conducted on a single-story, single-bay precast reinforced concrete structure made of plane parallel frames, i.e. that lacks secondary frames. Quasi-static and nonlinear time history analyses were performed to evaluate the BRFD efficacy in reducing seismic forces and displacements, and an importance analysis was carried out using a multi-criteria decision-making (MCDM) approach to identify the optimal configuration of the BRFD for the case study. The main results highlight that introducing the BRFD positively influences the dynamic performance of the structure, producing a significant reduction of interstorey drift and total base shear and preventing structural and non-structural damage.

1. Introduction

Precast RC structures have been widely used in industrial and commercial buildings since the 60 s in the most developed countries. These structural systems consist of modular, quickly installable, mass-produced elements that cover large spans. During those decades of economic growth, buildings were constructed without considering seismic design criteria, resulting in designs that only accounted for gravity loads.

Precast RC structures often face a significant seismic risk in earthquake-prone areas due to the lack of effective connection between structural elements. This issue was highlighted in the 2000 FIB report, which emphasised the combined effect of high seismic vulnerability and exposure in such structures [1]. This was confirmed during the 2012 Emilia Earthquake [2–7], which occurred in one of the most important industrial areas in Italy. Thousands of buildings in the region were designed without seismic detailing and collapsed during the seismic event, resulting in 28 casualties and hundreds of injured and displaced people, affecting the regional economy with enormous losses. It is evident that seismic losses resulting from buildings' structural damage impact society, the environment, and the industrial and commercial activities within the epicentral area [8]. The seismic retrofit of precast RC structures is essential to prolong their service life and mitigate seismic losses. The most common solutions involve traditional and passive control techniques based on energy dissipation.

Traditional retrofitting techniques, like concrete or steel jacketing and fibre-reinforced polymer (FRP) wrapping, are usually adopted to increase the structural elements' strength, especially the columns [9]. In

* Corresponding author.
E-mail addresses: eleonora.grossi@unife.it (E. Grossi), matteo.zerbin@unife.it (M. Zerbin), alessandra.aprile@unife.it (A. Aprile), raffaele.derisi@bristol.ac.uk (R. De Risi), flavia.deluca@bristol.ac.uk (F. De Luca).

https://doi.org/10.1016/j.istruc.2024.106960
Received 29 November 2023; Received in revised form 10 May 2024; Accepted 19 July 2024
Available online 1 August 2024

addition, external bracings are added to increase global stiffness [10,11] and steel connections are placed between structural elements to improve their connectivity [9]. Adopting traditional techniques requires the execution of additional works at the foundation level and, in case of significant seismic events, can still substantially damage the structure.

Passive control techniques primarily rely on the yielding or friction properties of metallic materials to dissipate seismic energy [12]. Implementing dissipative devices has proven to be an effective and affordable solution compared to traditional retrofitting methods, preventing damage to structural and non-structural elements [13]. During the last decade, several authors have focused on the seismic rehabilitation of precast RC structures, developing devices that are able to dissipate energy and simultaneously improve the connection between structural elements. Most of these solutions are intended to be installed as beam-to-column joints in the main frames, and the main damping principle relies on the friction and yielding properties of metallic materials. Eldin et al. [14] introduced a beam-to-column connection that dissipates energy using the linear sliding mechanism of a friction damper (FD). The studies of Huang et al. [15] focused on a bolted web FD and, to increase the stiffness of the system and the associated energy dissipation, the authors suggested the adoption of friction pads with added grooves. Valente [16] worked on a Rotational Friction Damper (RFD) that dissipates energy thanks to the subsequent opening and closing of the gap between the beam and the column during the seismic event. Colajanni et al. [17] conducted additional studies on RFDs by incorporating a bolted web FD into the solution suggested by Valente [16] to improve the damping capability of the system. Martinelli and Mulas [18] revised the layout of beam-to-column joints, and their solution was improved by Belleri et al. [19] by introducing a re-centring component. Pollini et al. [20] and Huang et al. [21] worked on devices whose damping mechanism is based on the yielding of steel tubes with added confinement elements to avoid instabilities during the yielding process. Bressanelli et al. [22] focused on the design and optimisation of a crescent moon steel element.

These devices proved to be very efficient in terms of energy dissipation and base shear reduction without limiting the buildings' usable surface area, which is an important aspect when considering the typical use of those buildings. As these devices are monodirectional, additional devices are essential on the plane orthogonal to the main frames to get energy dissipation in all the structure's directions as required by the seismic actions. However, additional devices cannot be inserted when orthogonal beams do not efficiently connect the parallel main frames.

Passive control techniques are known to have less environmental impact when compared to traditional techniques [23,24], especially if the adopted devices are easily restorable and can survive several shocks without damage. This is confirmed in the recent work of Cavalieri et al. [25], which computed a significant reduction of CO_2 emissions when retrofitting precast RC structures using innovative solutions instead of traditional ones.

The need for a dissipative device that can improve the overall seismic performance of a precast RC structure and has a low architectonical and environmental impact led the authors to develop a bidirectional damping device installed as a beam-to-column joint. This device unifies the concepts of RFDs and a movable plate system, obtaining a so-called Bidirectional Rotational Friction Damper (BRFD) that produces a damping effect along two main directions [26]. Furthermore, the device's ability to dissipate energy through friction enables it to remain undamaged during multiple seismic events while maintaining its damping capacity.

The present work shows the conceptualisation study of the BRFD to assess the feasibility and effectiveness of this innovative solution by a multi-criteria decision-making (MCDM) approach [27]. Conceptualisation studies are often used as proof-of-concept tools when introducing innovative solutions and are usually characterised by a simplified analytical and numerical characterisation of the object of study [28].

This paper is divided into six sections. Section 2 explains the layout of the BRFD and how it is expected to impact the structure, while Section 3 provides a simplified analytical model of the device. In Section 4, the properties of a precast RC structure are presented as a case study, and the influence of the BRFD on the frame's structural behaviour is highlighted. A sensitivity analysis is carried out in Section 5, and an importance analysis using a multi-criteria decision-making (MCDM) approach is conducted to identify the optimal BRFD configuration for the case study. Finally, Section 6 summarises the main findings and provides concluding remarks.

2. The BRFD layout and its structural impact

The BRFD is obtained by assembling layered steel plates, combining RFDs and a movable plate system to achieve a bidirectional behaviour. Fig. 1(a) shows an axonometric view of the BRFD, while Fig. 1(b) shows an example of its installation within one of the main portal frames at a 45° inclination angle from the existing beam as a beam-to-column joint. In the following, lowercase letters indicate the local reference system of the BRFD and, in general, of an element, while uppercase letters indicate the global reference system of the structure. It is worth noting that the plane generated by the BRFD's local *x*- and *y*-axis is inclined at 45° and perpendicular to the global *XZ* plane. Furthermore, the connection braces are hinged to the existing beam and column to allow the rotations around the global *Y* axis only and the deformations along the BRFD local *x* axis.

Core plates are the primary components of BRFD and are held together with four preload stud bolts. In each core plate's ends, friction pads are interlocked and kept in contact by the pressure generated by the stud bolts; as the device activates, the core plates' ends rotate around the stud bolts, and the friction pads slide on each other, dissipating energy and obtaining the deformed shapes of Fig. 2. A general displacement can be decomposed into a longitudinal component Δ_x and a transversal component Δ_y. Consequently, the BRFD's activation force has two components: a longitudinal component $F_{act,x}$ (local *x*-direction) and a transversal component $F_{act,y}$ (local *y*-direction). Two alignment guides with slotted holes are placed at the top and bottom of the device to keep preload bolts aligned with the central bolt, ensuring controlled displacements.

When introducing the BRFD inside a precast RC frame, the static scheme of the columns is expected to change from cantilever (Figs. 3(a) and 3(c)) into double-fixed element (Figs. 3(b) and 3(d)), resulting in a structural stiffness increment in both in-plane and out-of-plane frame's directions (see Fig. 3).

Three main conditions drive the BRFD design:

1. BRFD's steel elements shall not enter the plastic domain;
2. RC beams and columns shall not slide on each other during seismic motion, especially when a mechanical fastening is not installed (like in many pre-seismic code constructions);
3. RC beams and columns shear demand shall not exceed the capacity, while columns shall not yield.

3. The BRFD simplified analytical model

The analytical model here implemented aims to describe the BRFD behaviour using a simplified approach. As previously mentioned, the energy dissipation results from the relative rotation of the friction surfaces around the stud bolts, which maintain them coupled with each other. Assuming the circular contact area of Fig. 4, the relative motion between two surfaces begins when the interface sliding moment $M_{s,i}$ is reached:

$$M_{s,i} = \int_{\rho=R_i}^{R_e} \int_{\theta=0}^{2\pi} \rho^2 \frac{\mu F_P}{\pi\left(R_e{}^2 - R_i{}^2\right)} d\rho d\theta = \frac{2}{3}\mu F_P \frac{R_e{}^3 - R_i{}^3}{R_e{}^2 - R_i{}^2} \quad (1)$$

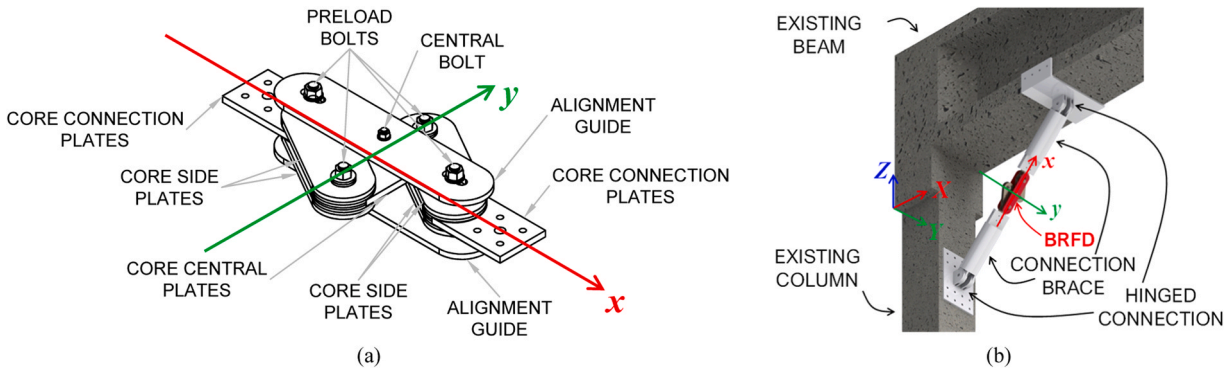

Fig. 1. BRFD (a) axonometric view and (b) example of installation as a beam-to-column joint.

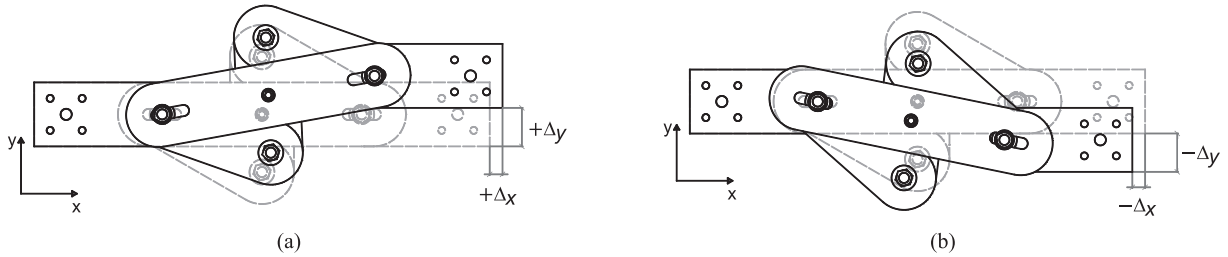

Fig. 2. BRFD bidirectional deformation shape in (a) tension ($+\Delta_x$ and $+\Delta_y$) and (b) compression ($-\Delta_x$ and $-\Delta_y$) configurations.

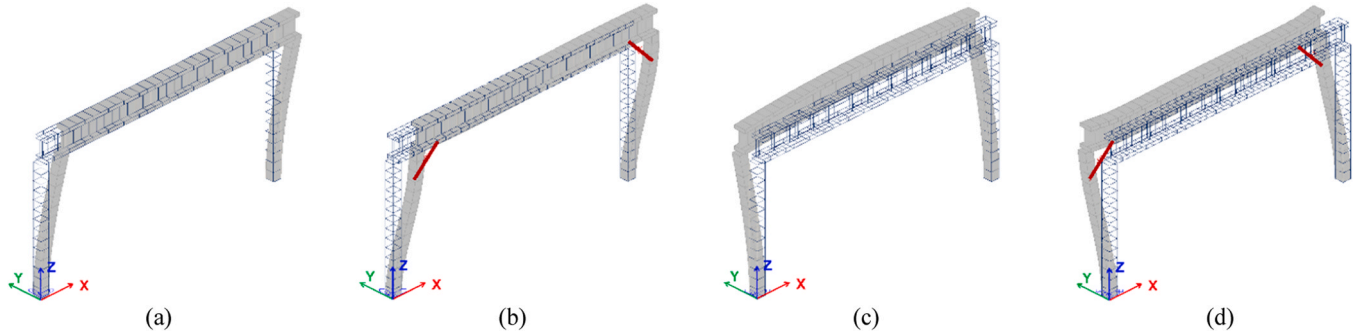

Fig. 3. Main frame deformation in X direction (a) without and (b) with BRFD, and deformation in Y direction (c) without and (d) with BRFD.

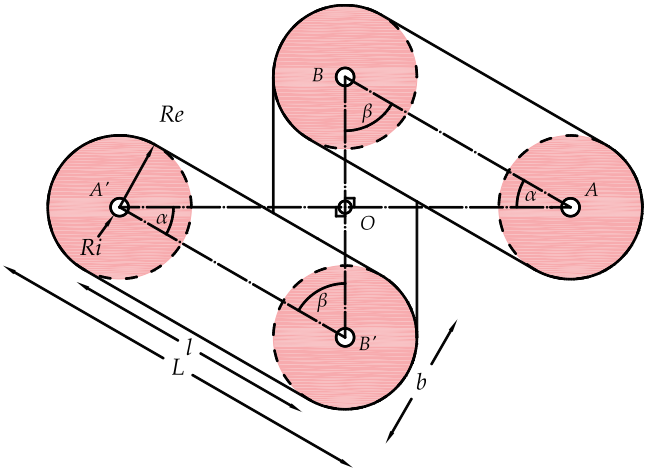

Fig. 4. BRFD core with circular contact areas highlighted in red colour.

where μ is the interface friction coefficient (here assumed constant to keep the model simple), F_P is the stud bolts axial load, R_e and R_i are outer and inner radius, respectively, and ρ and θ are the radial and angular coordinates [29].

The BRFD motion starts when the bending moment at nodes A, B, A' and B' of Fig. 4 equals the total sliding moment M_s expressed by Eq. (2), where $M_{s,i}$ is given by Eq. (1) and n is the number of sliding interfaces of the device's contact areas, depending on the plate's number.

$$M_s = nM_{s,i} \tag{2}$$

As a result, nodes A, B, A' and B' can be considered as rigid nodes when bending moment values are lower than M_s, and as hinged nodes for values equal to M_s.

This behaviour is statically reproduced using a rotational spring with a stiffness K_R that is highly stiff for bending moment values lower than M_s, and it is highly soft for bending moment values equal to M_s. Fig. 5(a) shows the static scheme associated with the BRFD core obtained by introducing the rotational springs. Nodes A, B, A' and B' are hinged and connected with beams of length $l = L - b$ (see Fig. 4), which represents the stud bolt's distance. Additionally, each node is equipped with a rotational spring of stiffness K_R, which replicates the rotational friction

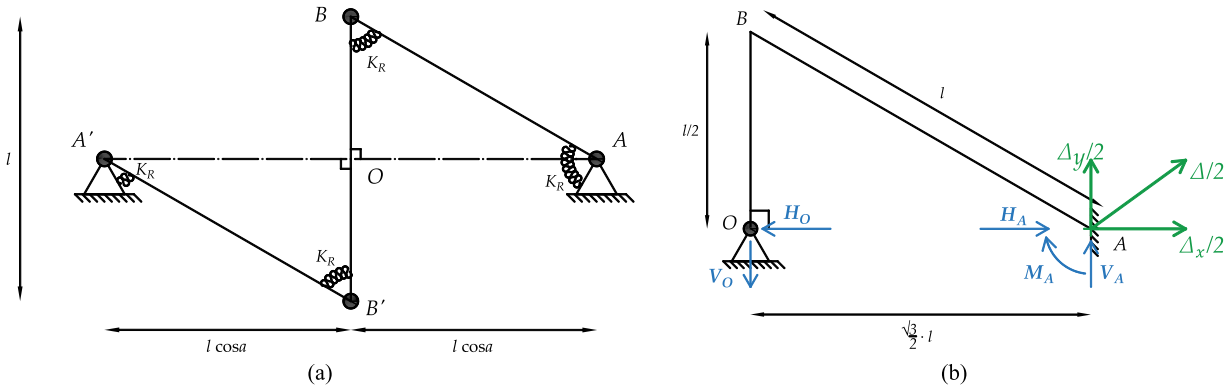

Fig. 5. BRFD core simplified static scheme (a) with rotational springs and (b) in the *before sliding* configuration.

behaviour.

To compute the relationship between the sliding moment M_s and the BRFD's activation forces, the configuration *before sliding* of Fig. 5(b) is considered in the following. As previously mentioned, nodes A, B, A' and B' can be considered as rigid nodes before sliding occurs while the alignment guides maintain the central symmetry around node O, allowing the static scheme of Fig. 5(a) to be transformed into the one of Fig. 5(b), analysing only the upper half. It is worth noting that, because of the central symmetry, when analysing the half BRFD, the displacements are halves with respect to the overall BRFD displacements, while the forces are equal to the overall BRFD forces.

When a generic displacement $\frac{\vec{\Delta}}{2} = \frac{\overrightarrow{\Delta_x}}{2} + \frac{\overrightarrow{\Delta_y}}{2}$ is applied to node A in the *before sliding* configuration of Fig. 5(b), the reaction forces H_O, V_O, H_A, V_A and M_A are generated on nodes O and A, respectively. More precisely, the reaction forces H_A, V_A and M_A coincide with the forces transferred by the BRFD into the existing structures. If $\Delta_s/2$ is the generic displacement that generates the moment M_s on nodes A and/or B, then H_A and V_A are equal to the longitudinal and transversal components ($F_{act,x}$ and $F_{act,y}$, respectively) of the activation force of the BRFD.

To better understand the mechanical behaviour of the BRFD, longitudinal ($\Delta_x/2$) and transversal ($\Delta_y/2$) displacements are studied separately. This allows to focus on the relationship between the sliding moment M_s and the activation forces and initial stiffness of the BRFD. In addition, to maintain the analytical model simple, only flexural deformation is considered in the analysis.

3.1. Longitudinal behaviour

When the BRFD is subjected to longitudinal displacements ($\Delta_x/2$), the static scheme of Fig. 5(b) can be simplified into the one of Fig. 6(a). A is a rigid node that can slide along x-directions, while O is a hinged node. When a longitudinal force F_x is applied to node A, the displacement $\Delta_x/2$ occurs and the reaction forces H_O, V_O, V_A and M_A are generated. It is worth noting that in the half BRFD analysed, the displacements are halves with respect to the overall BRFD displacements, while the forces are equal to the overall BRFD forces.

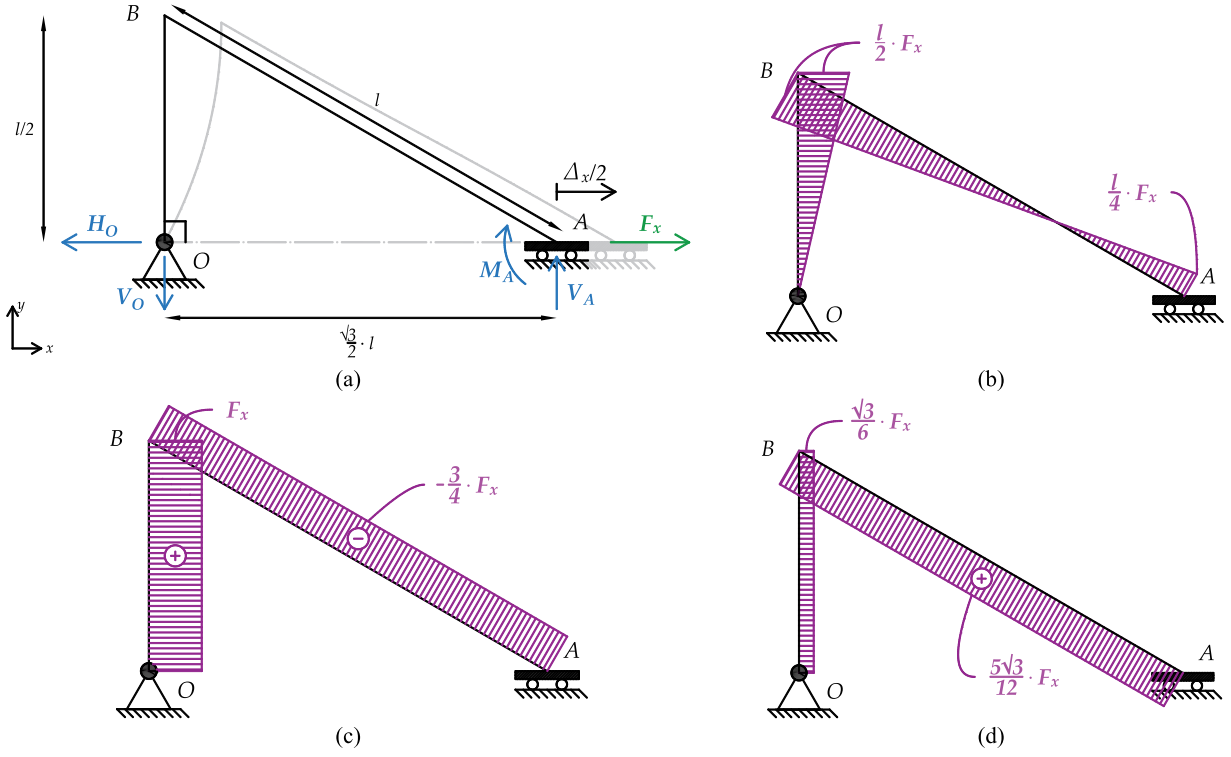

Fig. 6. BRFD's longitudinal component (a) static scheme, (b) bending moment, (c) shear and (d) axial forces diagrams.

The static scheme of Fig. 6(a) is one-time hyperstatic and has been analytically resolved by applying the Principle of Virtual Works (PVW). Figs. 6(b), 6(c) and 6(d) report, respectively, the obtained diagrams of bending moment, shear and axial forces. Node B reaches the higher value of bending moment (M_B), consequently when longitudinal displacement occurs, the BRFD activates when $M_B = M_s$. The relationship between M_s and the longitudinal activation force $F_{act,x}$ is described as follows:

$$F_{act,x} = \frac{2M_s}{l} \tag{3}$$

The displacement $\Delta_x/2$ is computed by applying the PVW and the initial longitudinal stiffness K_x is obtained from the ratio between F_x and Δ_x:

$$K_x = \frac{F_x}{\Delta_x} = \frac{E}{l^3}\left(\frac{1}{12I_{\overline{OB}}} + \frac{1}{8I_{\overline{BA}}}\right)^{-1} \tag{4}$$

where $I_{\overline{OB}}$ and $I_{\overline{BA}}$ are the moments of inertia of $\overline{OB}$ and $\overline{BA}$ elements (see Fig. 5(b)), which represent the core central and core side plates, respectively. $I_{\overline{OB}}$ and $I_{\overline{BA}}$ are computed by considering the whole cross-section of the elements; however, when designing the BRFD, the capacity of its elements is evaluated by considering the presence of the holes to avoid any risk of exceeding the elastic limit. To maintain the analytical model as general as possible, $I_{\overline{OB}}$ and $I_{\overline{BA}}$ are kept independent to each other: in the real device, core central and core side plates have a different stratification, and they can have a different geometry, which affects $I_{\overline{OB}}$ and $I_{\overline{BA}}$ inertia. However, when core central and core side plates have the same section, Eq. (4) can be written as follows:

$$K_x = \begin{cases} \frac{48}{7}\frac{EI}{l^3} & \text{for } n = 2 \quad \rightarrow I_{\overline{OB}} = I; I_{\overline{BA}} = 2I \\ 12\frac{EI}{l^3} & \text{for } n = 4 \quad \rightarrow I_{\overline{OB}} = 2I; I_{\overline{BA}} = 3I \end{cases} \tag{5}$$

From Eq. (5) it can be observed that when incrementing the number of friction interfaces and, consequently, the number of core's plates, the initial stiffness K_x increments as well.

3.2. Transversal behaviour

When the BRFD is subjected to transversal displacements ($\Delta_y/2$), the static scheme of Fig. 5(b) can be simplified into the one of Fig. 7(a). A is a rigid node that can slide along y-directions, while O is a hinged node. When the tansversal force F_y is applied to node A, the displacement $\Delta_y/2$ occurs and the reaction forces H_O, V_O, H_A and M_A are generated. It is worth noting that in the half BRFD is analysed, the registered displacements are halves with respect to the overall BRFD displacements, while the registered forces are equal to the overall BRFD forces.

The static scheme of Fig. 7(a) is one-time statically indetermined and has been analytically resolved by applying the PVW. Figs. 7(b), 7(c) and 7(d) report, respectively, the obtained diagrams of bending moment, shear and axial forces. Node A reaches the higher value of bending moment (M_A), consequently, when transversal displacement occurs, the BRFD activates when $M_A = M_s$. The relationship between M_s and the transversal activation force $F_{act,y}$ is described as follows:

$$F_{act,y} = \frac{2\sqrt{3}}{3}\frac{M_s}{l} \tag{6}$$

The displacement $\Delta_y/2$ is computed by applying the PVW and the initial longitudinal stiffness K_y is obtained from the ratio between F_y and Δ_y:

$$K_y = \frac{F_y}{\Delta_y} = \frac{E}{l^3}\left[\frac{1}{16k^2 I_{\overline{OB}}} + \frac{2}{I_{\overline{BA}}}\left(\frac{1}{4k} - \frac{1}{2}\right)^2\right]^{-1} \tag{7}$$

where $I_{\overline{OB}}$ and $I_{\overline{BA}}$ are the moments of inertia of $\overline{OB}$ and $\overline{BA}$ elements (see Fig. 5(b)), which represent core central and core side plates respectively, and $k = I_{\overline{BA}}/(2I_{\overline{OB}}) + 1$ is an non-dimensional parameter introduced to compact the formulation. $I_{\overline{OB}}$ and $I_{\overline{BA}}$ are computed by considering the whole cross-section of the elements; however, when designing the BRFD, the capacity of its elements is evaluated by considering the

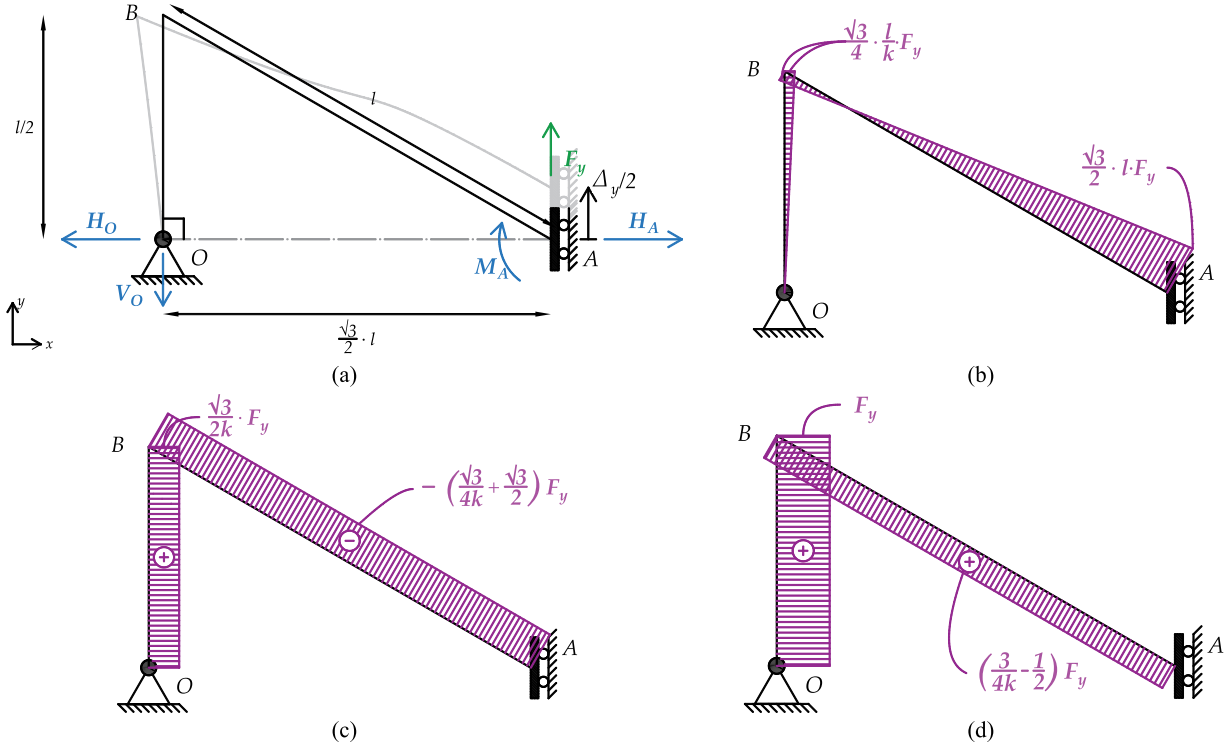

Fig. 7. BRFD's transversal component (a) static scheme, (b) bending moment, (c) shear and (d) axial forces diagrams.

presence of the holes to avoid any risk of exceeding the elastic limit. To maintain the analytical model as general as possible, $I_{\overline{OB}}$ and $I_{\overline{BA}}$ are kept independent to each other: in the real device, core central and core side plates have a different stratification and they can have a different geometry, which affect their inertia. However, when core central and core side plates have the same section, Eq. (7) can be written as follows:

$$K_y = \begin{cases} \frac{32}{5}\frac{EI}{l^3} & \text{for } n=2 \quad \rightarrow I_{\overline{OB}} = I; I_{\overline{BA}} = 2I; k = 2 \\ \frac{21}{2}\frac{EI}{l^3} & \text{for } n=4 \quad \rightarrow I_{\overline{OB}} = 2I; I_{\overline{BA}} = 3I; k = 7/4 \end{cases} \tag{8}$$

From Eq. (8) it can be observed that when incrementing the number of friction interfaces and, consequently, the number of core plates, the initial stiffness K_y increments as well.

3.3. Bidirectional behaviour

When the BRFD is subjected to a generic displacement $\frac{\overrightarrow{\Delta}}{2} = \pm\frac{\overrightarrow{\Delta_x}}{2} \pm \frac{\overrightarrow{\Delta_y}}{2}$, the reaction forces and the internal forces diagrams of Fig. 5(b) are computed by combinig the solutions of §3.1 and §3.2. More precisely, Eq. (9) represent the reaction forces when Δ_x and Δ_y are applied with the same and opposite sign, while Eq. (10) represent the condition that F_x and F_y shall satisfy to reach the sliding moment M_s at nodes A and B at the same time.

$$\begin{cases} H_A = H_O = \pm F_x \pm \frac{\sqrt{3}}{2k} F_y \\ V_A = V_O = \pm\frac{\sqrt{3}}{6} F_x \pm F_y \end{cases} \text{for} \frac{\overrightarrow{\Delta}}{2} = \pm\frac{\overrightarrow{\Delta_x}}{2} \pm \frac{\overrightarrow{\Delta_y}}{2} \tag{9}$$

$$\begin{cases} M_B = \pm\frac{l}{2} F_x \pm \frac{\sqrt{3}}{4k} l F_y = \pm M_s \\ M_A = \mp\frac{l}{4} F_x \mp \frac{\sqrt{3}}{2} l F_y = \mp M_s \end{cases} \text{for} \frac{\overrightarrow{\Delta}}{2} = \pm\frac{\overrightarrow{\Delta_x}}{2} \pm \frac{\overrightarrow{\Delta_y}}{2} \tag{10}$$

If F_x and F_y satisfy the condition of Eq. (10), the dimensionless interaction domain of Fig. 8 is obtained. The blue dots indicate a monodirectional loading condition, the orange dots indicate a loading condition with Δ_x and Δ_y applied with the same sign, and the green dots indicate a loading condition with Δ_x and Δ_y applied with the opposite sign.

The interaction domain of Fig. 8 is rectangular and indicates that the activation forces of the BRFD remain constant and equal to the monodirectional conditions of §3.1 and §3.2, independently from the loading direction. This behaviour permits considering the longitudinal and transversal components of the BRFD as unrelated, allowing the definition of a simplified uncoupled hysteretic behaviour.

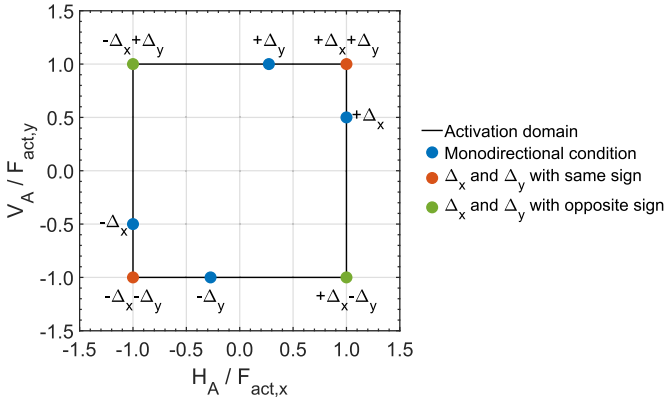

Fig. 8. Activation forces dimensionless domain.

3.4. The simplified hysteresis cycles

One of the main hypotheses of the simplified analytical model for the BRFD is that the nodes associated with the dissipative areas can be considered as hinged nodes once the device activates (see Fig. 4). As a result, when the BRFD is subjected to the longitudinal force $F_{act,x}$, which activates the kinematic along the local x-direction, the rigid node B becomes a hinged node (see Fig. 9(a)). Similarly, when the BRFD is subjected to the transversal force $F_{act,y}$, which activates the kinematic along the local y-direction, the rigid node A becomes a hinged node (see Fig. 9(b).

When longitudinal displacement occurs, the bending moment around node B equals M_s and, because of the friction mechanism, it cannot increase. The relationship between M_s and the longitudinal activation force $F_{act,x}$ is described as follows:

$$F_{act,x}(\Delta\beta) = \frac{2M_s}{l \bullet \cos\Delta\beta} \tag{11}$$

where $\Delta\beta$ is the angle $\overline{OB}$ element generates with its original position when moving. The distance between nodes B and O changes when the BRFD activates along the longitudinal direction, becoming $l/2\cos\Delta\beta$.

When transversal displacement occurs, the bending moment of node A equals M_s and, because of the friction mechanism, it cannot increase. Moreover, the relationship between M_s and $F_{act,y}$ is given by Eq. (6), since the distance between nodes A and O keeps equal to $\sqrt{3}/2l$ when the BRFD activates along the transversal direction.

Fig. 10 shows the shape of the two hysteresis cycles associated with BRFD's longitudinal (blue line) and transversal (red line) components (x- and y-direction, respectively). The shapes are obtained by combining the Eqs. (4), (11) and (5) for the longitudinal component, and Eqs. (6) and (7) for the transversal component.

The BRFD's hysteresis cycle associated with its longitudinal component exhibits a force increment when incrementing the displacement. This increment is a function of $\cos\Delta\beta$, but for small displacement Δ_x, typical of seismic devices real use condition, the increment can be assumed as linear. The BRFD's hysteresis cycle associated with its transversal component exhibits a force constancy when incrementing the displacement. It is worth noting that the two components are unrelated and independent of each other. This behaviour simplifies the numerical implementation of the BRFD, as it can be defined as a link with two separated hysteresis laws, one for each component.

The presented analytical model assumes a constant friction coefficient μ, according to Coulomb's law. For instance, the shapes of Fig. 10 can be significantly affected by the real μ behaviour during the real use conditions. This topic may be critical and will be the focus of further research after the execution of mechanical testing. In fact, the here presented simplified analytical model is useful to understand the BRFD's influence when implemented inside a precast RC structure, which is the main goal of the present work.

4. Case study and BRFD influence

To evaluate the influence of the BRFD on a structure's behaviour during a seismic event, a case study is conducted on a single-story, single-bay precast reinforced concrete structure, whose geometry is represented in Fig. 11. Main frames (shown in Fig. 11(b)) consist of 7 m height square columns and 15 m length prestressed I-shaped beams connected by three 15 m length prestressed PI-shaped slabs. The total weight of the case study is 1393 kN, which averages a mass of 14 tons. It is worth noting that the prestressed PI-shaped slabs cannot be considered a proper connection between the two parallel main frames (X direction); as a result, the case study lacks secondary frames (Y direction).

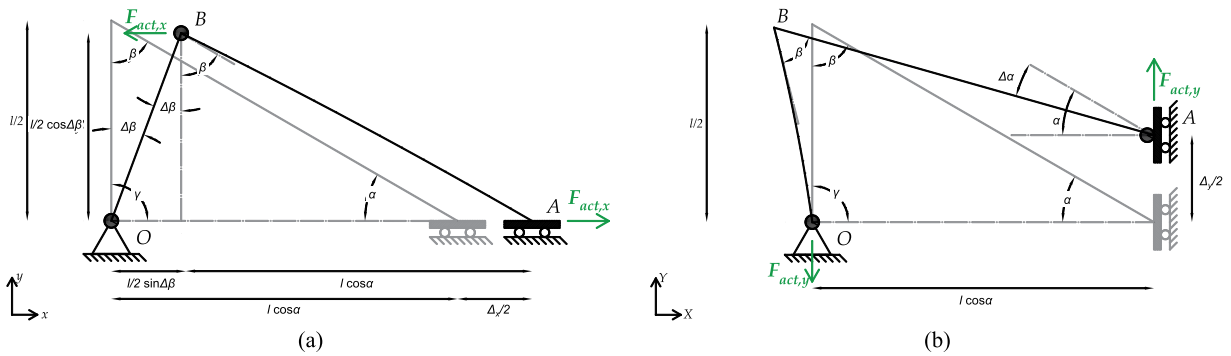

Fig. 9. BRFD core simplified kinematics when (a) longitudinal and (b) transversal displacements occur.

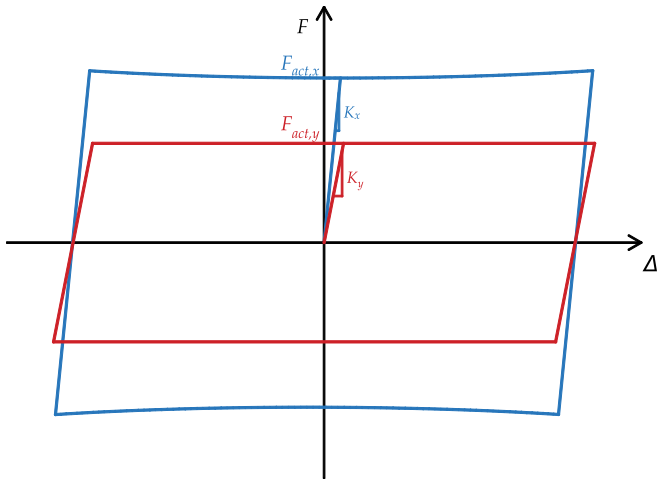

Fig. 10. Longitudinal and transversal components of the BRFD's simplified analytical hysteresis cycles.

Fig. 12 shows the reinforcement detailing of columns and beams, while the material properties were assessed by on-site sampling: the concrete has a cylindrical compressive strength of 38 MPa and a Young modulus of 33 GPa, reinforcing steel bars have a yielding stress of 544 MPa and a Young modulus of 200 GPa, prestressed steel bars have a yielding stress of 1670 MPa and a Young modulus of 200 GPa.

Given the absence of proper out-of-plane frames in the *Y* direction, the BRFD is only inserted inside the main frames in the *X* direction, as shown in Fig. 1(b).

The case study was numerically implemented in Opensees [30] using the scheme of Fig. 13 and STKO [31] as pre- and post-processor. I-shaped beams are modelled as *elastic beams* hinged at the ends, while square columns are *fibre sections* with a fixed base. To validate the numerical implementation of the columns, the relationship between the bending moment (*M*) and the curvature (χ) was analytically computed and compared with the numerical one in Fig. 14(a). The comparison highlights the good matching between analytical and numerical previsions, validating the adopted modelling approach. The roof is simulated with a *diaphragm constrain* type in *X-Y* plane using a control node at the centre of the roof.

The BRFDs are modelled using *ZeroLength* links with two different *Steel01* materials along their local *x* and *y* directions to describe the two components of the BRFD hysteretic laws described in Section 3. More precisely, the BRFD longitudinal component *x* aligns with the axial

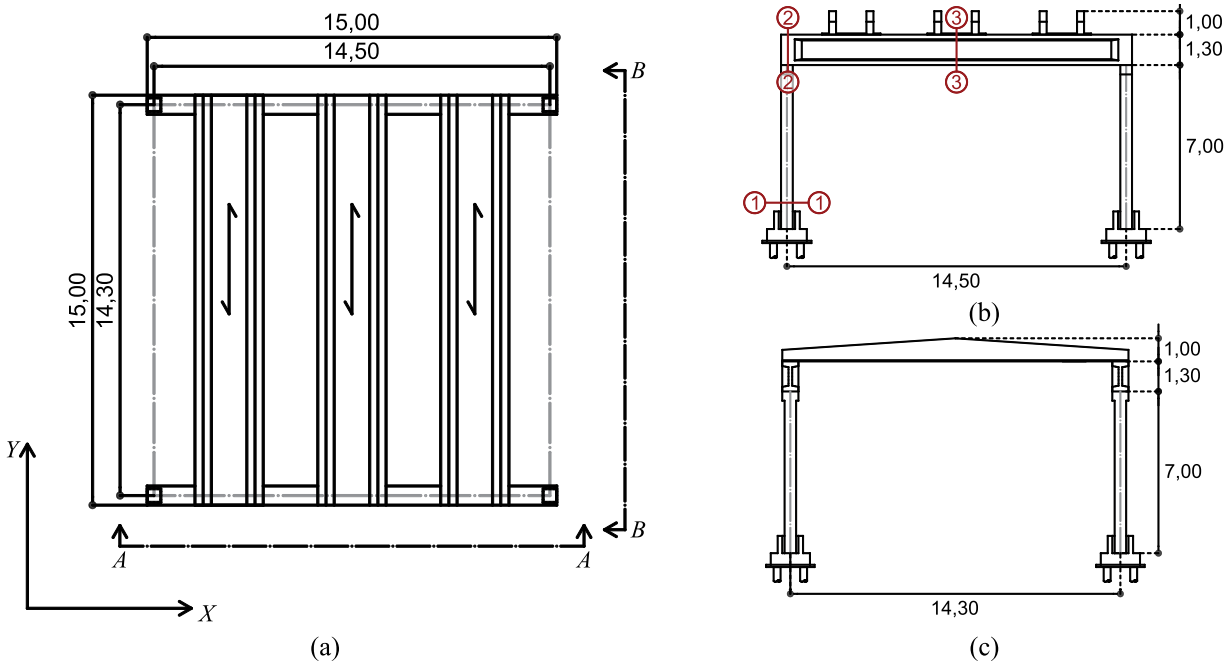

Fig. 11. Precast RC structure used as a case study: a) top view, b) *A-A* view and c) *B-B* view. Dimensions in m.

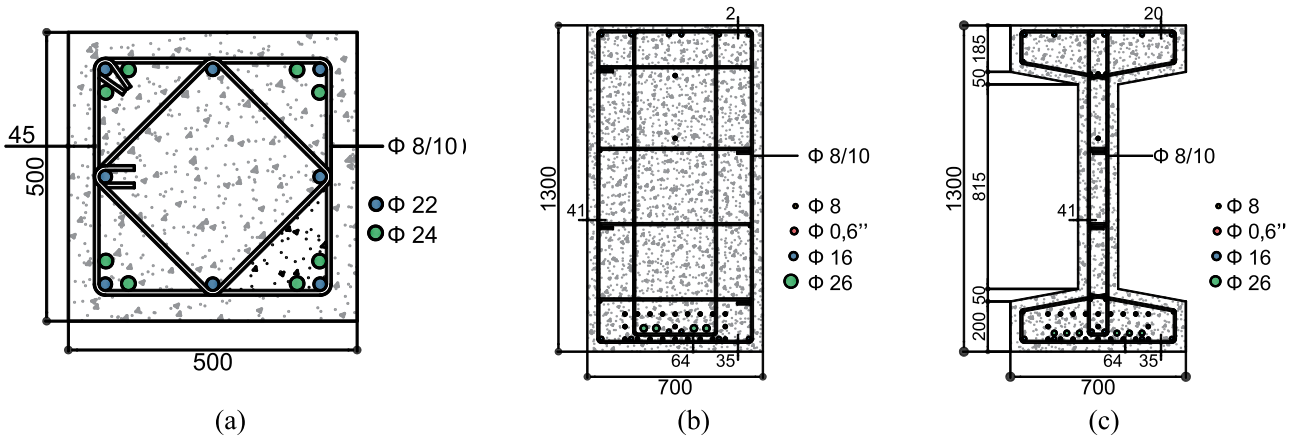

Fig. 12. Elements detailing: a) column base (Sections 1–1), b) beam end (Sections 2–2) and c) beam centre (Sections 3–3). Dimensions in mm.

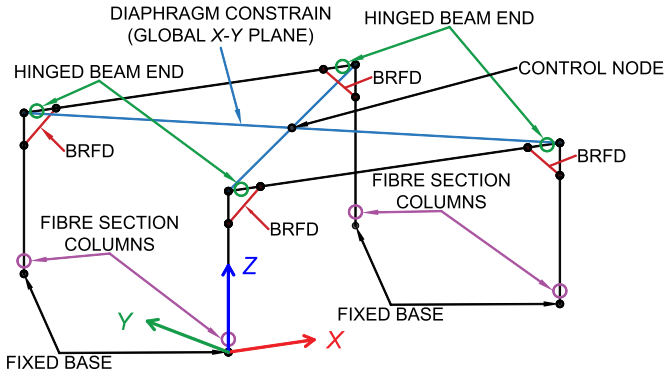

Fig. 13. Numerical implementation scheme of the case study.

direction of the *ZeroLength* links, and the BRFD transversal component *y* aligns with the global *Y* direction. Figs. 14(b) and 14(c) compare the analytical (A tag) and the numerical (N tag) previsions of the BRFD longitudinal and transversal components, respectively. The comparison highlights the good matching between analytical and numerical previsions in both longitudinal (*x*) and transversal (*y*) directions, validating the adopted modelling approach.

4.1. Quasi-static performance without and with BRFD

A quasi-static analysis was performed to preliminarily evaluate the influence of the BRFD when installed inside the case study. The control node located at the top of the structure (see Fig. 13) was subjected to a sinusoidal displacement law with an amplitude of ± 300 mm, a frequency of 0.05 Hz for three cycles and a time step increment of 0.001 s

Three different frames have been modelled: F0, which represents the case study without the BRFDs, F1, which represents the case study that implemented a beam-to-column connection with the elastic properties of the BRFDs, and F2, which represents the case study that implemented a beam-to-column connection with the hysteretic properties of the BRFDs. It is worth noting that F1 resembles a traditional retrofit executed by introducing a steel connection between the structural elements and it is used, together with F0, as a reference for a better understanding of the nonlinear behaviour of F2.

Table 1 describes the properties of the implemented frames in terms of linear elastic period along directions *X* and *Y*, $T_{0,X}$ and $T_{0,Y}$ respectively, and BRFD's properties in terms of activation forces along its local *x*- and *y*-direction, $F_{act,x}$ and $F_{act,y}$ respectively, and initial stiffness along its local *x*- and *y*-direction, K_x and K_y respectively. The values of the BRFD properties reported in Table 1 come from the results of §5.2 and are here used as an example. It is worth noting that the presence of the BRFD decreases the elastic period of the case study by about 45 % in both *X* and *Y* directions. This is because the BRFD elastic stiffness increases the rigidity of the beam-to-column node, causing the columns

Table 1
Description of the three implemented frames and BRFD's properties.

Frame	Description	$T_{0,X}$ [s]	$T_{0,Y}$ [s]	$F_{act,x}$ [kN]	$F_{act,y}$ [kN]	K_x [kN/m]	K_y [kN/m]
F0	No BRFD	0.77	0.77	-	-	-	-
F1	BRFD elastic properties	0.44	0.41	-	-	$1{\cdot}10^6$	$9{\cdot}10^5$
F2	BRFD hysteretic properties	0.44	0.41	125	72	$1{\cdot}10^6$	$9{\cdot}10^5$

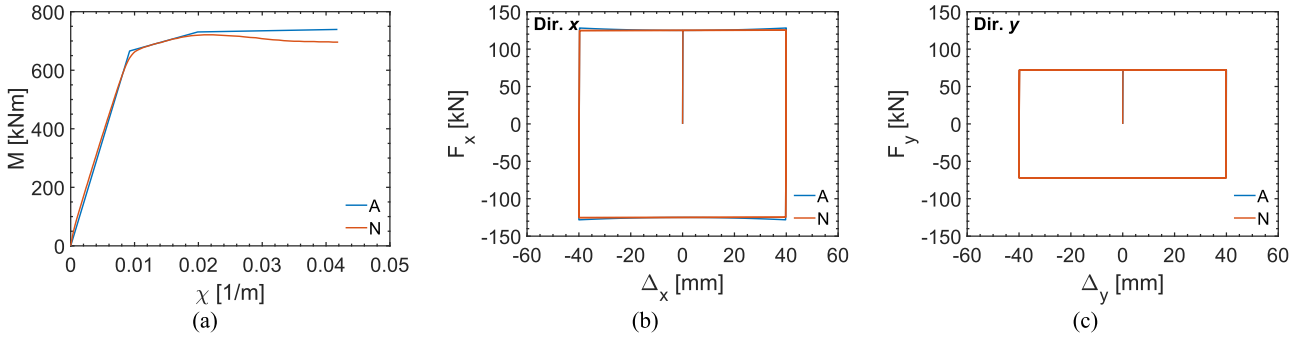

Fig. 14. Comparison between analytical (A) and numerical (N) previsions in terms of (a) columns $M-\chi$ relationship and BRFD $F-\Delta$ relationship along its (b) longitudinal *x* and (c) transversal *y* directions.

static scheme to change from cantilever into double-fixed elements. This is quite a general outcome, whenever the beam-to-column joints are strengthened using additional steel plates. However, the stiffening effect may be different depending on the specific structural layout.

Fig. 15 shows the results of the quasi-static analysis in terms of top displacement and total base shear relationship in directions X and Y, Figs. 15(a) and 15(b) respectively. F0 exhibits a similar hysteresis cycle in the X and Y direction due to the steel yielding at the square columns footings; this similarity is due to the frame's square plant and the symmetric detailing of the columns (see Fig. 12(a)). F1 exhibits a higher stiffness than F0, with higher forces and smaller displacement associated with the columns yielding. Furthermore, the hysteresis cycle in the X direction differs from the one in the Y direction; this difference is caused by the dissimilar changes in the frame's static scheme that the BRFDs induce in the two global directions. More precisely, the column goes from a cantilever to a fixed scheme along the X direction and from a cantilever to a semi-fixed scheme along the Y direction. In fact, the columns yield simultaneously at the base and the top sections in the X direction, while in the Y direction, the columns yield firstly at the base and then at the top section. F2 combines the behaviours of F0 and F1: F2 exhibits the same stiffness as F1 until the BRFD activates, then behaves more similarly to F0, registering a similar hysteresis cycle in the X and Y direction.

The BRFD positively influences the case study's structural behaviour, unaltering the top displacement associated with the column yielding and slightly increasing the related total base shear. Moreover, when the BRFD activates, it restores the original static scheme of the structure, allowing the columns to behave as cantilevers.

5. Dynamic performance

To investigate the benefits of the BRFD on the case study during a seismic event, Nonlinear Time History Analyses (NLTHAs) were performed on frames F0, F1 and F2 using natural ground motions. Seven pairs of ground motions were selected from the European Strong Motion database [32]; the ground motions are spectrum-compatible for a high seismic area in Italy (i.e. L'Aquila [33]) and are scaled to match the Life-Safety limit state assuming soil type B and Importance Class III according to Eurocode 8–1 [34]. Table 2 summarises the properties of the selected ground motions, including the original Peak Ground Accelerations (PGA) ad Scale Factors (SF) in x and y directions.

NLTHA were performed in Opensees [30] using STKO [31] and Matlab [35] as pre- and post-processing tools. The results are assessed considering the total base shear (Fb), interstorey drift (IDR), columns' base rotation and shear utilisation factors ($\rho_{C,\theta}$ and $\rho_{C,V}$), and equivalent damping (ξ_{eq}). The columns' utilization factors are a-dimensional and are defined as follows:

$$\rho_{C,\theta} = \frac{\theta_{Ed}}{\theta_y} \tag{12}$$

$$\rho_{C,V} = \frac{V_{Ed}}{V_{Rd}} \tag{13}$$

Columns' utilisation factors are computed as a ratio between demand and capacity: values lower than 1 indicate the satisfaction of the columns' safety checks. The rotation capacity was set as the rotation associated with the base column yielding θ_y computed according to Eurocode 8–3 [36], while the shear capacity as the shear associated with the shear failure V_{Rd} computed according to Eurocode 8–3 [36]. It is worth noting that when defining $\rho_{C,\theta}$, the choice to associate the capacity rotation with the yielding rotation of the column was driven by one of the main objectives of this work, which is to avoid structural damage to the building.

The equivalent damping ξ_{eq} is computed from the acceleration spectrum in ADRS (Acceleration-Displacement Response Spectrum) format [37] once the top displacement and total base shear demand are determined.

5.1. Sensitivity analysis

To investigate the effects of the BRFD's activation forces ($F_{act,x}$ and $F_{act,y}$) and initial stiffnesses (K_x and K_y) on the case study during a seismic event, the F2 frame was subjected to a sensitivity analysis.

The analytical model developed in Section 3 allows to describe $F_{act,y}$ as a function of $F_{act,x}$ and K_y as a function of K_x as follow:

$$F_{act,y} = \frac{2\sqrt{3}M_s}{3l} = \frac{\sqrt{3}}{3}F_{act,x} \tag{14}$$

$$K_y = \begin{cases} \frac{32}{5}\frac{EI}{l^3} = \frac{14}{15}K_x \cong 0.93K_x \approx 0.9K_x & \text{for } n = 2 \\ \frac{21}{2}\frac{EI}{l^3} = \frac{7}{8}K_x \cong 0.88K_x \approx 0.9K_x & \text{for } n = 4 \end{cases} \tag{15}$$

Eqs. (14) and (15) are obtained by merging Eq. (3) with (6) and Eq. (5) with (8), respectively.

When performing the sensitivity analysis, $F_{act,x}$ and K_x varied as a function of the BRFD feasibility while $F_{act,y}$ and K_y were computed according to Eqs. (14) and (15). Considering the BRFD feasibility, $F_{act,x}$ was set to range between 25 and 250 kN, while K_x between 10^5 and 10^6 kN/m. The main objective of this sensitivity analysis is to identify the $F_{act,x}$-K_x couple which better improves the case study performance under the selected seismic action.

Fig. 16 summarises the sensitivity analysis results in terms of $\rho_{C,\theta}$, $\rho_{C,V}$, IDR and ξ_{eq} as mean values of the NLTHA with seven ground motions for each $F_{act,x}$-K_x couple. The response levels are expressed using different colours, as shown on the scaling bar of each graph. In the graphs associated with $\rho_{C,\theta}$ and $\rho_{C,V}$ (Figs. 16(a) and 16(b) respectively), green shades are associated with the satisfaction of the columns' safety checks, while red shades corresponds to unsatisfactory columns' safety checks. In the graph associated with IDR (Fig. 16(c)), the darker blue

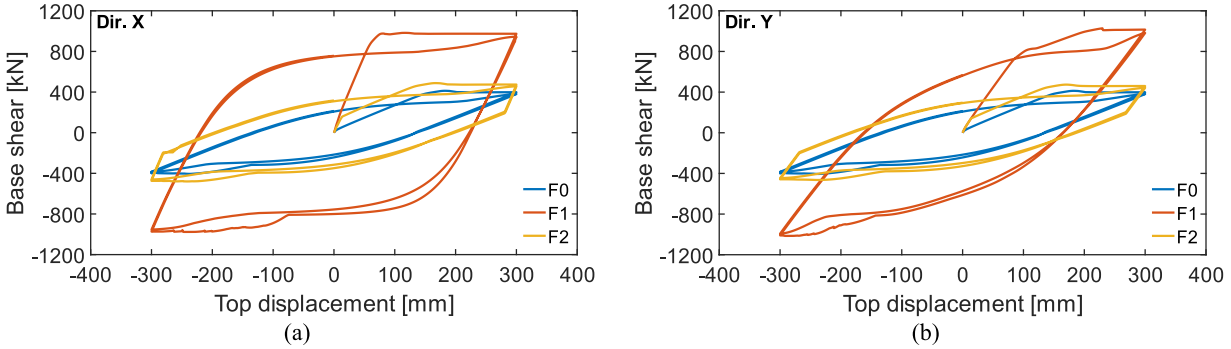

Fig. 15. Quasi-static performance using a cyclic displacement law along (a) X and (b) Y direction.

Table 2
Properties of the selected ground motions.

TH n°	Earthquake event	Station ID	Magnitude (Richter scale)	EC8 soil class	Original PGA x [g]	Original PGA y [g]	SF x	SF y
1	Central Italy (24/08/2016)	PZI1	6.0	B	0.05	0.05	8.65	8.49
2	Central Italy (30/10/2016)	MZ24	6.6	C	0.76	1.02	0.38	0.51
3	Central Italy (26/10/2016)	NOR	5.9	B	0.21	0.12	1.82	3.24
4	Friuli 1st shock (06/05/1976)	TLM1	6.4	B	0.32	0.35	1.24	1.11
5	Emilia 2nd shock (29/05/2012)	T0819	5.5	C	0.26	0.25	1.52	1.56
6	Umbria Marche 2nd shock (26/09/1997)	CSA	6.0	C	0.11	0.17	3.70	2.27
7	Emilia 1st shock (20/05/2012)	MRN	6.1	C	0.26	0.26	1.49	1.48
Average values			6.1		0.28	0.32	2.68	2.67

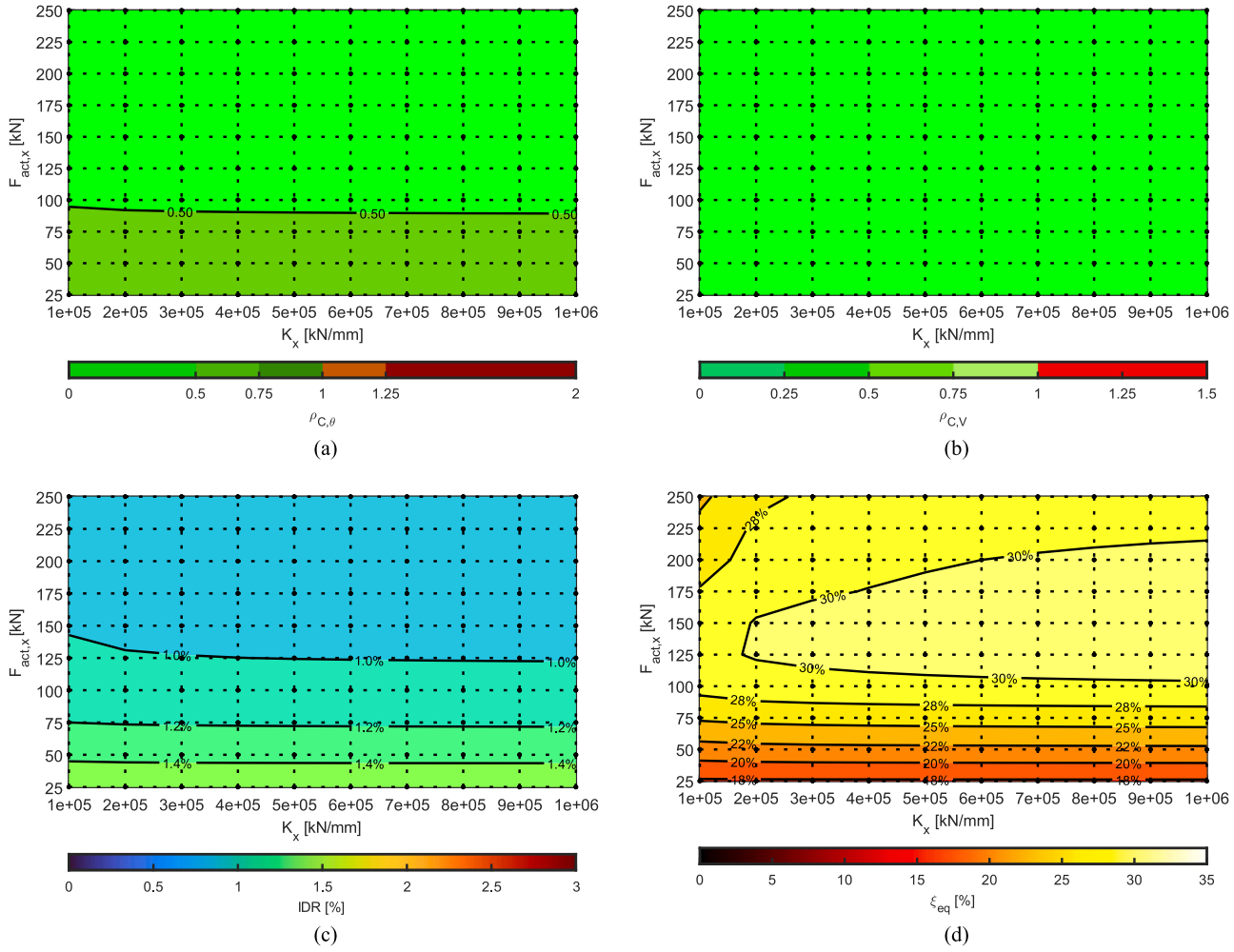

Fig. 16. Sensitivity analysis results in terms of (a) column rotation and (b) shear factors, (c) interstorey drifts and (d) equivalent damping.

colour shades indicate lower interstorey drift values, which are usually associated with a lower damage level [38]. In the graph associated with ξ_{eq} (Fig. 16(d)), the lighter yellow colour shades indicate higher equivalent damping values, which are associated with a better overall performance of the BRFD.

When incrementing $F_{act,x}$ values, F2 performance improves and exhibits a decrement in column base rotations and interstorey drifts: for $F_{act,x}$ values higher than 100 kN, $\rho_{C,\theta}$ are lower than 0.50, and IDR are lower than 1 %. However, when incrementing $F_{act,x}$ values, F2 exhibits an increment of total base shear, which may affect the columns' shear check and the equivalent damping. This behaviour is typical of additional damping systems and has been observed by several authors [39–42]. It is worth noting that the columns' shear failure V_{Rd} is 196 kN, which is quite a high value and leads to $\rho_{C,V}$ lower than 0.50 for all the investigated $F_{act,x}$-K_x combinations. As a result, in this case, the increment of total base shear is insignificant, but it is a critical aspect to be considered, especially when the columns' detailing is poor for the shear capacity.

When incrementing K_x, F2 performance improves (especially when associated with higher $F_{act,x}$ values) and exhibits an increment of equivalent damping: for K_x higher than $5{\cdot}10^5$ kN/m and $F_{act,x}$ values between 100 and 200 kN, ξ_{eq} is higher than 30 %.

The sensitivity analysis highlights that, for a better improvement of F2 dynamic performance, $F_{act,x}$ ideal values range between 100 and 200 kN, while $K_x$ideal values are higher than $5{\cdot}10^5$ kN/m.

5.2. Importance analysis using a multi-criteria decision-making (MCDM) approach

To better identify the optimal configuration of the BRFD for the case study, an importance analysis using a multi-criteria decision-making (MCDM) approach was conducted. The adopted approach uses the entropy-right method to consider the multiple-factors effect of columns' safety checks ($\rho_{C,\theta}$ and $\rho_{C,V}$) and performance parameters (IDR and ξ_{eq}) to identify the most important $F_{act,x}$-K_x couple in terms of F2 overall performance. The details of the adopted approach can be found in the work of Guo et al. [27].

The importance indexes are divided into two groups: the first one considers the columns' safety checks associated with rotation and shear factors ($\rho_{C,\theta}$ and $\rho_{C,V}$, respectively), the second group considers the overall F2 performance in terms of interstorey drift and equivalent damping (IDR and ξ_{eq} respectively). These parameters are firstly standardised as non-dimensional parameters, then combined according to the entropy-right method. Each importance index is associated with a weight that comprehends an objective weight, which is a function of the entropy, and a subjective expert-based weight λ. In this work, the selected groups are assumed to have the same importance, which results in equal λ values following the hierarchy scheme of Fig. 17.

The comprehensive indexes are finally obtained by combining the standardised importance indexes with the comprehensive weight: the $F_{act,x}$-K_x couple with the highest comprehensive index is the most important and resembles the optimal solution.

Fig. 18 shows the results of the importance analysis in terms of performance level from "Really good" (white colours) to "Really bad" (red colours) with an additional area associated with "BRFD unfeasible" (black region). This additional area is obtained considering BRFDs with maximum length of 90 cm with μ equal to 0.45, according to previous authors findings [43–45], and the $F_{act,x}$ values that are effectively obtainable from the geometry associated with each K_x. In fact, lower values of K_x are associated with smaller BRFD's plate width and a smaller range of available studs' diameters and applicable torque. As a result, higher values of $F_{act,x}$ are not reachable for the lower K_x values.

F2 exhibits the best performance when $F_{act,x}$ ranges between 100 and 150 kN and K_x is higher than $6{\cdot}10^5$ kN/m (see the white area of Fig. 18), confirming the remarks concerning the sensitivity analysis of §5.1. More precisely, the MCDM approach suggests a solution with $F_{act,x}$ equals to 125 kN and K_x equals to 10^6 kN/m as the most important, i.e., the optimal BRFD configuration.

It is worth noting that, $F_{act,x}$ values have a major impact on the obtained performance level than K_x values. In fact, while a change in the initial stiffness K_x maintains the performance level mainly unaltered, a change in activation force $F_{act,x}$ may result in a significant modification of the performance level. Since the activation force is strictly related to the axial tension of the preload stud bolts (see Eq. (1) and Fig. 1(a)), during the actual design of the BRFD this force can be optimised by varying the torque applied to preload bolts.

The optimal BRFD configuration identified using the MCMD approach represents the case study when located in the site selected at the beginning of §5. A change in the structure or the site location can affect the obtained results and the optimal BRFD configuration.

5.3. Dynamic performance without and with BRFD

To investigate the benefits of the BRFD on the dynamic response of the case study during a seismic event, NLTHA were performed on frames F0, F1 and F2 using natural ground motions. F1 and F2 frames were modelled, implementing the characteristics of Table 1, using the BRFD optimal configuration properties.

Fig. 19 compares the dynamic performance of F0, F1 and F2 in terms of Fb, IDR, $\rho_{C,\theta}$ and $\rho_{C,V}$ as mean values of the NLTHA with seven ground motions. Given the frame's square plant and the symmetric detailing of the columns, the response of F0 and F2 in the X direction resembles the one in the Y direction; on the contrary, the response of F1 in the X direction differs from the one in the Y direction, especially in terms of displacements, confirming what already highlighted in §4.1.

F0 results indicate that while the shear checks are perfectly satisfied with $\rho_{C,V}$ values lower than 0.5 (see Fig. 19(d)), the damage registered by the columns is quite significant. In fact, $\rho_{C,\theta}$ values are higher than 1 (see the red line of Fig. 19(c)), and IDR values are higher than 2 %, usually associated with high damage of structural and non-structural elements [38] (see the black line of Fig. 19(b)).

F1 results indicate an overall performance improvement, with $\rho_{C,\theta}$ and $\rho_{C,V}$ values lower than 1, and IDR values lower than 1 %. However, Fb values exhibit an average increment of 64 % with respect to F0. While in this case study, the structural response is not affected by this increment, limiting the total base shear increment is a good practice, especially for structures with poor shear detailing. Despite the total base increment, F1 avoids panels and structural damage (red and black lines of Fig. 19(b)).

F2 exhibits the best overall performance improvement, with $\rho_{C,\theta}$ and $\rho_{C,V}$ values lower than 1, and IDR values lower than 1 %. Moreover, Fb values exhibit an average decrement of 28 % with respect to F0. It can be

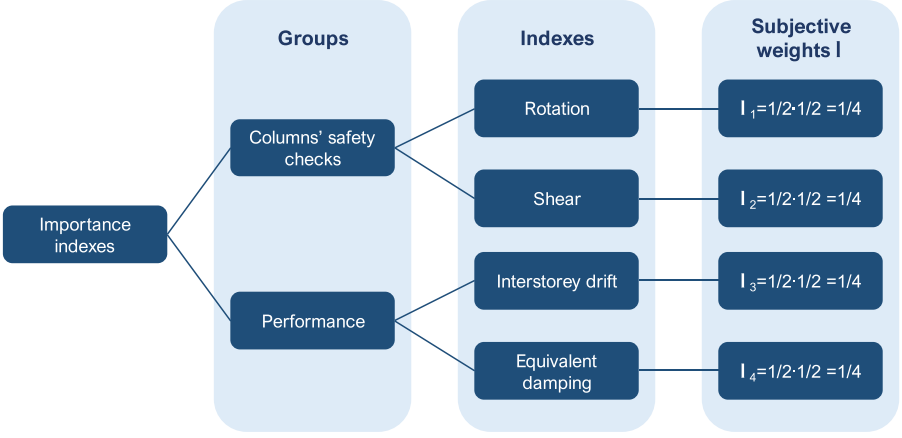

Fig. 17. Subjective weights adopted in the importance analysis.

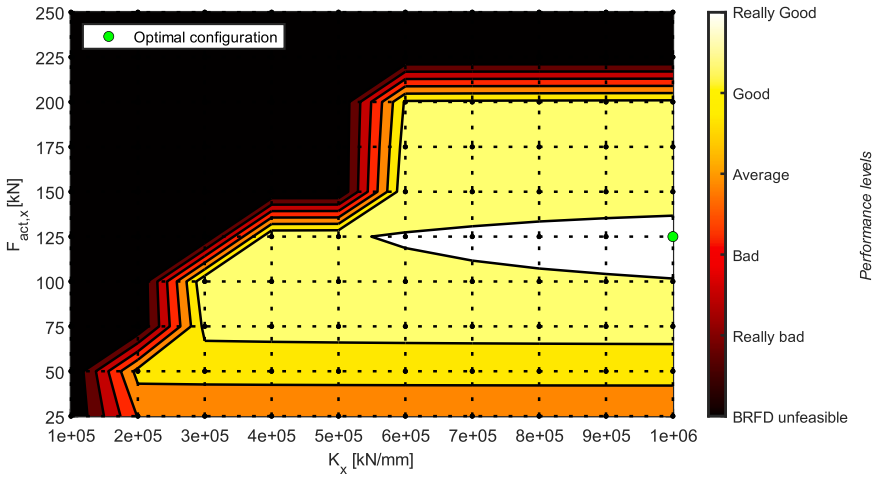

Fig. 18. Performance level map considering only the feasible BRFD configurations.

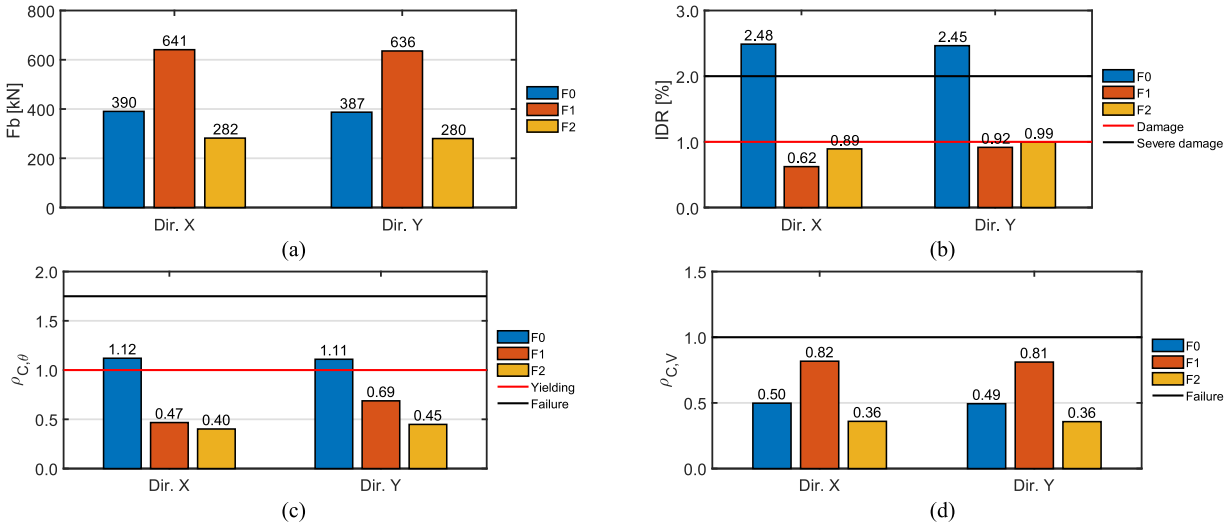

Fig. 19. F0, F1 and F2 dynamic performance: (a) total base shear, (b) interstorey drift, (c) column rotation and (d) shear factors.

confirmed that F2 results in a particularly effective solution that combines the satisfaction of the columns' safety checks and an average 62 % decrement of IDR without a significant alteration of the existing structural system, avoiding structural and non-structural damage (red and black lines of Fig. 19(b)).

6. Conclusions

The present work shows the conceptualisation study of an innovative seismic protection device called Bidirectional Rotational Friction Damper (BRFD) for precast RC structures with poor connections. The BRFD behaves as a beam-to-column joint and damper at once; the device unifies the concepts of Rotational Friction Dampers and movable plate geometry, producing a damping effect along two main directions. This is a relevant characteristic because, up to date, the existing damping devices produce a damping effect in one direction only. Furthermore, the device's ability to dissipate energy through friction enables it to remain undamaged during multiple seismic events while maintaining its damping capacity.

The BRFD behaviour is described as a combination of two components, a longitudinal (local x direction) and a transversal (local y direction) one, identifying an activation force ($F_{act,x}$ and $F_{act,y}$) and an initial stiffness (K_x and K_y) for each one.

To evaluate the influence of the BRFD on a structure's behaviour during a seismic event, a case study is conducted on a single-story, single-bay precast RC structure that lacks secondary frames, allowing the implementation of BRFD inside the main frames only. Quasi-static and nonlinear time history analyses were performed on the case study, identifying three different frames: F0, which represents the case study without BRFDs, F1, which represents the case study with the elastic properties of the BRFD, and F2, which represents the case study with the hysteretic properties of the BRFD.

To identify the optimal configuration of the BRFD for the case study, a sensitivity analysis was carried out on F2, performing an importance analysis using a multi-criteria decision-making (MCDM) approach.

The main findings are summarised in the following:

- The simplified analytical model indicates that the two behaviours in the two directions are unrelated and independent. Moreover, the hysteresis cycles can be described using a bilinear hysteretic law. This behaviour simplifies the numerical implementation of the BRFD, as it can be defined as a link with two separated hysteresis laws, one for each component.
- The quasi-static analysis shows that the BRFDs application positively influence the case study's structural behaviour, unaltering the top displacement associated with the column yielding and slightly increasing the related total base shear. Moreover, when the BRFDs

activate, the original static scheme of the structure is restored, allowing the columns to behave as cantilevers.

- The sensitivity analysis performed on F2 highlights that the dynamic performance better improves when the activation force ranges between 100 and 200 kN for $F_{act,x}$ and between 58 and 115 kN for $F_{act,y}$, and when the initial stiffness is higher than $5{\cdot}10^5$ kN/m for K_x and higher than $4{\cdot}10^5$ kN/m for K_y.
- The importance analysis performed using the MCDM approach suggests that the optimal BRFD configuration is obtained when $F_{act,x} = 125$ kN, $F_{act,y} = 72$ kN, $K_x = 10^6$ kN/m and $K_y = 9{\cdot}10^5$ kN/m.
- The introduction of the BRFD positively benefits the case study's dynamic performance, significantly reducing interstorey drift (62 %) and a reduction of total base shear (28 %) without altering the existing structural scheme, avoiding structural and non-structural damage.

Obviously, the dynamic results of the present work are representative of the case study when located in the site selected at the beginning of §5. Since the obtained results are dependent on both the structural layout and location site hazard, the MCMD approach can be proposed as an effective design tool for the BRFD sizing.

As a summary, the conceptualisation analysis performed on BRFD highlights that such a system can effectively improve a precast RC structure's behaviour during seismic events. However, further research is needed to fully develop the potential of the device. More precisely, future studies will be focused on the execution of bidirectional mechanical tests on a real-scale prototype, the development of a numerical model which includes a friction law that considers the influence of sliding velocity, pressure and temperature, and topological studies to investigate the effects on multi-span and multi-storey buildings.

CRediT authorship contribution statement

Matteo Zerbin: Conceptualization, Methodology, Resources, Supervision, Validation, Writing – review & editing. **Alessandra Aprile:** Conceptualization, Funding acquisition, Methodology, Project administration, Resources, Supervision, Validation, Writing – review & editing. **Eleonora Grossi:** Conceptualization, Data curation, Formal analysis, Investigation, Software, Visualization, Writing – original draft. **Raffaele De Risi:** Data curation, Formal analysis, Methodology, Software, Writing – review & editing. **Flavia De Luca:** Methodology, Project administration, Supervision, Validation, Writing – review & editing.

Declaration of Competing Interest

The authors declare the following financial interests/personal relationships which may be considered as potential competing interests: Eleonora Grossi has patent #102020000013738/2021 issued to Italian Patent and Trademark Oce, Ministry of Economic Development. Alessandra Aprile has patent #102020000013738/2021 issued to Italian Patent and Trademark Oce, Ministry of Economic Development. Matteo Zerbin has patent #102020000013738/2021 issued to Italian Patent and Trademark Oce, Ministry of Economic Development.

Acknowledgements

The authors wish to acknowledge the support provided by the University of Ferrara: "Bidirectional Friction Links for Seismic Retrofit of Existing Precast RC Structures (FAR2078914)", "A friction damper for seismic retrofit of precast RC structures" (FAR2151302), "Experimental testing of innovative friction dampers for seismic retrofit of precast RC structures" (FAR22718675). The authors wish also to acknowledge the support provided by FIRD funding from the Engineering Department of the University of Ferrara, year 2022: "Mechanical and tribological testing of a novel damping device for seismic risk mitigation of industrial buildings" (2022-FAR.L-FIRD_DE_AA_001).

References

[1] vol. 27. Lausanne: International Federation for Structural Concrete (fib),; 2003.
[2] Bournas DA, Negro P, Taucer FF. Performance of industrial buildings during the Emilia earthquakes in Northern Italy and recommendations for their strengthening. Bull Earthq Eng 2014;12. https://doi.org/10.1007/s10518-013-9466-z.
[3] Grimaz S, Malisan P. Near field domain effects and their consideration in the international and Italian seismic codes. Boll Di Geofis Teor Ed Appl 2014;55:717–38. ⟨https://doi.org/10.4430/bgta0130⟩.
[4] Magliulo G, Ercolino M, Petrone C, Coppola O, Manfredi G. The emilia earthquake: seismic performance of precast reinforced concrete buildings. Earthq Spectra 2014;30. https://doi.org/10.1193/091012EQS285M.
[5] Casotto C, Silva V, Crowley H, Nascimbene R, Pinho R. Seismic fragility of Italian RC precast industrial structures. Eng Struct 2015;94:122–36. https://doi.org/10.1016/J.ENGSTRUCT.2015.02.034.
[6] Ercolino M, Magliulo G, Manfredi G. Failure of a precast RC building due to Emilia-Romagna earthquakes. Eng Struct 2016;118:262–73. https://doi.org/10.1016/j.engstruct.2016.03.054.
[7] Demartino C, Vanzi I, Monti G, Sulpizio C. Precast industrial buildings in Southern Europe: loss of support at frictional beam-to-column connections under seismic actions. Bull Earthq Eng 2018;16. https://doi.org/10.1007/s10518-017-0196-5.
[8] Batalha N, Rodrigues H, Varum H. Seismic performance of RC precast industrial buildings—learning with the past earthquakes. Innov Infrastruct Solut 2019;4. https://doi.org/10.1007/s41062-018-0191-y.
[9] Belleri A, Torquati M, Riva P, Nascimbene R. Vulnerability assessment and retrofit solutions of precast industrial structures. Earthq Struct 2015;8:801–20. https://doi.org/10.12989/eas.2015.8.3.801.
[10] Cao X-Y, Shen D, Feng D-C, Wang C-L, Qu Z, Wu G. Seismic retrofitting of existing frame buildings through externally attached sub-structures: State of the art review and future perspectives. J Build Eng 2022;57:104904. https://doi.org/10.1016/j.jobe.2022.104904.
[11] Cao X, Wu G, Feng D, Wang Z, Cui H. Research on the seismic retrofitting performance of RC frames using SC-PBSPC BRBF substructures. Earthq Eng Struct Dyn 2020;49:794–816. https://doi.org/10.1002/eqe.3265.
[12] Christopoulos C, Filatrault A. Principles of passive supplemental damping and seismic isolation. Pavia, Italy: IUSS Press,; 2006.
[13] Grossi E, Zerbin M, Aprile A. Advanced techniques for pilotis RC frames seismic retrofit: performance comparison for a strategic building case study. Buildings 2020;10:149. https://doi.org/10.3390/buildings10090149.
[14] Eldin MN, Dereje AJ, Kim J. Seismic retrofit of RC buildings using self-centering PC frames with friction-dampers. Eng Struct 2020;208. https://doi.org/10.1016/j.engstruct.2019.109925.
[15] Huang L, Zhou Z, Huang X, Wang Y. Variable friction damped self-centering precast concrete beam–column connections with hidden corbels: Experimental investigation and theoretical analysis. Eng Struct 2020;206:110150. https://doi.org/10.1016/j.engstruct.2019.110150.
[16] Valente M. Improving the seismic performance of precast buildings using dissipative devices (Elsevier Ltd) Procedia Eng 2013;vol. 54:795–804. https://doi.org/10.1016/j.proeng.2013.03.073.
[17] Colajanni P, La Mendola L, Monaco A, Pagnotta S. Design of RC joints equipped with hybrid trussed beams and friction dampers. Eng Struct 2021;227. https://doi.org/10.1016/j.engstruct.2020.111442.
[18] Martinelli P, Mulas MG. An innovative passive control technique for industrial precast frames. Eng Struct 2010;32. https://doi.org/10.1016/j.engstruct.2009.12.038.
[19] Belleri A, Marini A, Riva P, Nascimbene R. Dissipating and re-centring devices for portal-frame precast structures. Eng Struct 2017;150. https://doi.org/10.1016/j.engstruct.2017.07.072.
[20] Pollini AV, Buratti N, Mazzotti C. Behavior factor of concrete portal frames with dissipative devices based on carbon-wrapped steel tubes. Bull Earthq Eng 2021;19:553–78. https://doi.org/10.1007/s10518-020-00977-y.
[21] Huang W, Hu G, Miao X, Liu X, Xie H. Seismic performance of concrete-filled steel tube devices for precast concrete beam-column connections. J Mech Mater Struct 2021;16:63–88. https://doi.org/10.2140/JOMMS.2021.16.63.
[22] Bressanelli ME, Bosio M, Belleri A, Riva P, Biagiotti P. Crescent-moon beam-to-column connection for precast industrial buildings. Front Built Environ 2021;7. https://doi.org/10.3389/fbuil.2021.645497.
[23] Pomponi F, Moncaster A. Embodied carbon mitigation and reduction in the built environment – What does the evidence say? J Environ Manag 2016;181:687–700. https://doi.org/10.1016/j.jenvman.2016.08.036.
[24] Pomponi F, Moncaster A. Circular economy for the built environment: a research framework. J Clean Prod 2017;143:710–8. https://doi.org/10.1016/j.jclepro.2016.12.055.
[25] Cavalieri F, Bellotti D, Caruso M, Nascimbene R. Comparative evaluation of seismic performance and environmental impact of traditional and dissipation-based retrofitting solutions for precast structures. J Build Eng 2023;79:107918. https://doi.org/10.1016/j.jobe.2023.107918.
[26] Aprile A., Grossi E., Zerbin M. A Novel Friction Damper for Seismic Retrofit of Precast RC Structures with Poor Connections. In: Ilki Alper, Çavunt Derya, Selim Çavunt Yavuz, editors. fib Symposium 2023 - vol. 1, Istanbul: Springer - Lecture Notes in Civil Engineering (LNCE); 2023, p. 1384–1394. https://doi.org/10.1007/978–3-031–32519-9_140.

[27] Guo A, Liu Z, Li S, Li H. Seismic performance assessment of highway bridge networks considering post-disaster traffic demand of a transportation system in emergency conditions. Struct Infrastruct Eng 2017;13:1523–37. https://doi.org/10.1080/15732479.2017.1299770.
[28] Zhang Y, De Risi R, Alexander NA. A frictional sliding on a sprung slope (FSSS) device that axiomatically confers energy dissipation with re-centring to post-tensioned (PT) frames: A conceptual study. Eng Struct 2021;244. https://doi.org/10.1016/j.engstruct.2021.112794.
[29] Belleri A, Marini A, Riva P, Nascimbene R. Dissipating and re-centring devices for portal-frame precast structures. Eng Struct 2017;150. https://doi.org/10.1016/j.engstruct.2017.07.072.
[30] McKenna F. OpenSees: a framework for earthquake engineering simulation. Comput Sci Eng 2011;13:58–66. ⟨https://doi.org/10.1109/MCSE.2011.66⟩.
[31] Petracca M., Candeloro F., Camata G. STKO user manual. Pescara, Italy: 2017.
[32] EC. European Strong-Motion Database 2023. ⟨http://www.isesd.hi.is/⟩.
[33] NTC2018. Decreto ministeriale del 17 Gennaio 2018, Aggiornamento delle "Norme tecniche per le costruzioni". Italy: 2018.
[34] C.E.N. Eurocode 8: Design of Structures for Earthquake Resistance. Part 1: General rules, seismic actions and rules for buildings (UNI EN 1998–1). 2005.
[35] MathWorks. MATLAB 2022.
[36] C.E.N. Eurocode 8: Design of Structures for Earthquake Resistance. Part 3: Assessment and retrofitting of buildings (UNI EN 1998–3). 2011.
[37] Fajfar P. Capacity spectrum method based on inelastic demand spectra. Earthq Eng Struct Dyn 1999;28:979–93.
[38] Priestley MJN, Calvi GM, Kowalsky MJ. Displacement-based seismic design of structures. Pavia, Italy: IUSS Press: Distributed by Fondazione EUCENTRE,; 2007.
[39] Constantinou MC, Tsopelas P, Hammel W, Sigaher AN. TogglE-brace-damper Seismic Energy Dissipation Systems. J Struct Eng 2001;127. https://doi.org/10.1061/(ASCE)0733-9445(2001)127:2(105).
[40] Martínez-Rueda JE. On the evolution of energy dissipation devices for seismic design. Earthq Spectra 2002;18. https://doi.org/10.1193/1.1494434.
[41] Soong TT, Spencer BF. Supplemental energy dissipation: state-of-the-art and state-of-the-practice. Eng Struct 2002;24. https://doi.org/10.1016/S0141-0296(01)00092-X.
[42] Barzegar V, Laflamme S, Downey A, Li M, Hu C. Numerical evaluation of a novel passive variable friction damper for vibration mitigation. Eng Struct 2020;220. https://doi.org/10.1016/j.engstruct.2020.110920.
[43] Grossi E, Aprile A, Zerbin M. Tribological investigation on metal mating surfaces to explore real use conditions of a novel friction damper for seismic applications. Eng Struct 2023;278:115473. https://doi.org/10.1016/j.engstruct.2022.115473.
[44] Grossi E, Baroni E, Aprile A, Fortini A, Zerbin M, Merlin M. Tribological behavior of structural steel with different surface finishing and treatments for a novel seismic damper. Coatings 2023;13:135. https://doi.org/10.3390/coatings13010135.
[45] Grossi E, Aprile A, Zerbin M, Livieri P. Preliminary experimental tests of a novel friction damper for seismic retrofit of RC precast structures. Eng Sructures 2024;305:117718. https://doi.org/10.1016/j.engstruct.2024.117718.